ACADEMIC PRESS

Available online at www.sciencedirect.com
SCIENCE DIRECT®

Journal of Colloid and Interface Science 265 (2003) 409–421

JOURNAL OF
Colloid and
Interface Science

www.elsevier.com/locate/jcis

The effect of surfactant on the efficiency of shear-induced drop coalescence

Steven D. Hudson,[a,*] Alex M. Jamieson,[b] and Brian E. Burkhart [c]

[a] *Polymers Division, National Institute of Standards and Technology, Gaithersburg, MD 20899-8544, USA*
[b] *Department of Macromolecular Science and Engineering, Case Western Reserve University, Cleveland, OH 44106-7202, USA*
[c] *The Goodyear Tire & Rubber Co., Akron, OH 44305, USA*

Received 14 August 2002; accepted 9 April 2003

Abstract

The volume-averaged shear-induced drop-coalescence efficiency ε_v is measured by in situ videomicroscopy of blends of poly(propylene glycol) and poly(ethylene glycol), emulsified with poly(ethyleneglycol-*b*-propyleneoxide-*b*-ethyleneglycol) block copolymer surfactant. Adsorption of copolymer to the immiscible blend interface is indicated by a reduction in the interfacial tension, measured by the drop retraction method. The effects of temperature, copolymer molecular weight, copolymer concentration, and capillary number Ca are explored. At small Ca, ε_v is essentially independent of shear rate and drop size, and depends mainly on the solubility, diffusivity, and surface pressure of the surfactant, indicating that drop trajectories during flow are perturbed by surfactant Marangoni stresses that are controlled by the diffusion-limited *sorption* of surfactant. At larger Ca, ε_v approaches zero. This arrest of coalescence is associated with the onset of slight deformation of the drops during their collision, and *drainage* of a film of continuous fluid between them. The effect of the surfactant, though significant, saturates even while the amount of surfactant adsorbed to the interface is quite small. Governing dimensionless parameters, associated material parameters and the behavior of more insoluble surfactants are discussed.

Keywords: Coalescence; Adsorption; Surfactant; Emulsions; Drop collisions; Film drainage; Peclet; Marangoni

1. Introduction

Since it is often essential to control droplet size in emulsions, manipulation of the rate of coalescence is necessary. The ability of surfactants or block copolymers to influence drop breakup and coalescence phenomena during the mixing of immiscible fluids is well known and has great commercial importance, but the mechanism by which they achieve this remains obscure. Here, by determining the appropriate governing dimensionless parameters (see Table 1), we determine this mechanism (for soluble surfactants) in regimes of both low and moderate capillary number. Basic parameters are introduced in this section.

As two drops approach one another in flow, two effects determine the possibility of coalescence. First, the drop trajectories curve away from one another; hydrodynamic interactions that arise from the viscosity of the continuous fluid cause drops to repel one another, so that collisions may be avoided, even while the drops remain essentially undeformed [1]. "Collisions" are defined to occur when the distance between drop centers is less than or equal to the sum of their radii; smaller separations are possible if the collision force is strong enough to cause drop deformation in the near contact region. Such deformation may or may not be sufficient to prevent drop contact and coalescence: collided drops remain nearly in contact for a finite "interaction time," as the pair rotates in the flow, while a thin film of continuous fluid of thickness h separating the drops drains [2]. Film drainage is the second effect that decides whether two drops will coalesce or will ultimately be convected away from one another. These two processes have been discussed recently by Yang et al. [3].

A useful parameter that characterizes this film drainage process can be obtained by nondimensionalizing the thin-film force balance for glancing-angle collisions [4,5]. This and related so-called dimensionless Hamaker parameters implicitly define relevant length scales for film drainage: the drop radius a_{cr} at the onset of the importance of film drainage [5,6] and the final film thickness h_c before it rup-

* Corresponding author.
E-mail address: steven.hudson@nist.gov (S.D. Hudson).

0021-9797/$ – see front matter
doi:10.1016/S0021-9797(03)00396-5

Table 1
Summary of dimensionless parameters

Number	Definition
$\varepsilon_v = \frac{d\ln(a_v)}{dt}\frac{1}{\dot\gamma\phi_{\rm eff}}\frac{\pi}{4(2-2^{2/3})}$	Volume averaged coalescence efficiency, Eq. (3)
$\mathrm{Ca} = \eta_c\dot\gamma a_v/\sigma$	Capillary number
$Ma \approx \Pi/(\sigma_0\mathrm{Ca})$	Marangoni number
$Ma_{\rm eff} = Ma/(Ma_c + Ma)$	Parameter gauging the importance of Marangoni effects during thin film drainage, Eq. (18)
$a_v/a_{\rm cr} \approx \frac{1}{0.420}\big[\frac{1}{\hat\eta+1.02\ln(\hat\eta)+14.9}\big(\frac{\hat\eta(\hat\eta+2/3)}{\hat\eta+1}\big)^2\frac{\mathrm{Ca}^4\sigma a_v^2}{A}\big]^{1/6}$	The ratio of volume-averaged drop size to the predicted critical size for the onset of film drainage effects, Eq. (1) [5,6]
$Pe = \dot\gamma a_v^2/D$	(Bulk) Peclet number
$Pe_\sigma = \dot\gamma a_v^2/D_\sigma$	Interfacial Peclet number, Eq. (2)
$Pe_{\rm eff} = \frac{Pe_\sigma(HPe+\dot\gamma/k_d)}{Pe_\sigma+HPe+\dot\gamma/k_d}$	Effective Peclet number, accounting for diffusive and sorption processes, Eq. (14)
$Pe_{\sigma f} = \sigma_0 a_v\mathrm{Ca}^{3/2}/(\eta_d D_\sigma)$	Thin-film interfacial Peclet number, Eq. (17) [10]

tures [7]. In this report, we consider the volume-averaged drop radius a_v (of a not-too-polydisperse emulsion), because the larger drops are most susceptible to film formation. The ratio $a_v/a_{\rm cr}$ is an important dimensionless parameter describing whether or not film drainage is important [5],

$$a_v/a_{\rm cr} \approx \frac{1}{0.420}\left[\frac{1}{\hat\eta+1.02\ln(\hat\eta)+14.9}\times\left(\frac{\hat\eta(\hat\eta+2/3)}{\hat\eta+1}\right)^2\frac{\mathrm{Ca}^4\sigma a_v^2}{A}\right]^{1/6}, \qquad (1)$$

where A is the Hamaker parameter, σ is interfacial tension, the (volume-averaged) capillary number is $\mathrm{Ca} = \eta_c\dot\gamma a_v/\sigma$, η_c is the continuous-phase viscosity, the viscosity ratio is $\hat\eta = \eta_d/\eta_c$, η_d is the drop viscosity, and $\dot\gamma$ is the shear rate. The film radius b is approximately $(a_v\mathrm{Ca}^{1/2})$ [2]. The quantity $\hat\eta + 1.02\ln(\hat\eta) + 14.9$ arises from an approximation of drop mobility functions, evaluated in the limit of zero separation between drops [8]. $a_{\rm cr}$ thus defined is accurate within 1.5% for $0.1 \leqslant \hat\eta \leqslant 1$, for a broad range of shear stress and interfacial tension [5]. When a_v exceeds $a_{\rm cr}$, coalescence is reduced markedly, because the time required for drainage of the film to a thickness h_c exceeds the interaction time for a substantial fraction of drop collions [2,5,6].

Both drop trajectory and thin film drainage (and of course the coalescence efficiency derived from them) are controlled by the so-called "mobility" of the interface. This mobility is a function of two primary factors: the viscosity ratio $\hat\eta$ [1,2] and the presence of surfactant at the interface [9,10]. Recent experiments and calculations further suggest that interfacial slip may be a factor in immiscible polymers without surfactant [11].

When surfactant is present on the interface, motion of the interface can cause interfacial concentration gradients, which produce interfacial tension gradients that oppose, reduce, and perhaps prevent the motion. Reduction of the interface velocity need not occur if sorption or interfacial diffusion processes are fast enough to maintain uniform concentration, in spite of interfacial motion. If the surfactant is insoluble, adsorption and desorption do not occur and analysis of the interfacial surfactant transport equations,

$$\nabla_s[\Gamma u - D_\sigma\nabla\Gamma] = 0, \qquad (2a)$$

$$\nabla_s\big[\Gamma u - D_\sigma(d\Gamma/d\sigma)\nabla\sigma\big] = 0, \qquad (2b)$$

$$\nabla_s\big[u + a_v/(\eta Ma\,Pe_\sigma)\nabla\sigma\big] = 0, \qquad (2c)$$

yields $Ma\,Pe_\sigma$ as the governing dimensionless number [9,12]. Here, Γ is the interfacial concentration of surfactant, u is the interfacial velocity, $Ma = E/\mathrm{Ca}$ is the Marangoni number, $E = (-d\sigma/d\Gamma)\Gamma/\sigma$ is the Gibbs–Marangoni elasticity, D_σ is the interfacial diffusivity of the surfactant, $Pe_\sigma = \dot\gamma a_v^2/D_\sigma$ is the interfacial Peclet number (Table 1), and ∇ represents the gradient operator. We approximate $E \approx \Pi/\sigma_0$, where σ_0 is the bare interfacial tension without surfactant and Π is the interfacial pressure ($\Pi = \sigma_0 - \sigma$). Pe_σ governs the uniformity of interfacial concentration and Ma the stresses resulting from interfacial concentration gradients. At small values of this number $Ma\,Pe_\sigma$, the interface mobility is unaffected by the presence of surfactant, because either the interfacial concentration is uniform (diffusion dominates) or the surfactant layer is weak. At large values of this number, the Marangoni stress retards the interface with respect to motion of the drops either towards or away from each other [9,13].

Under different conditions, a parameter other than $Ma\,Pe_\sigma$ may govern interfacial mobility. For example, since different velocities and lengths are relevant for either drop trajectory or film drainage, different Peclet numbers will be defined in each case, as discussed in later sections (see Table 1). Furthermore, if surfactant sorption occurs during an appropriate time scale, a different parameter is relevant [14,15] (Table 1).

Coalescence phenomena are remarkably sensitive to minor changes in interfacial velocity effected by surfactants [10,16,17]. Such effects can be investigated either by direct examination of drop trajectories and film drainage times [3,16] or by analysis of the evolution of drop size distributions obtained from large populations of drops subjected to flow [18,19]. In the former case, drops can be subjected to different types of flow and can have a variety of starting positions on different streamlines. The distance between these streamlines is called the offset [3]. Coalescence

occurs when the offset and Ca are smaller than certain critical values. As the offset increases, the critical Ca decreases.

When the drop size distribution for large numbers of drops is studied in simple flows, all possible offset conditions are realized in the experiment, a great advantage for determining the coalescence efficiency. Thus, at a given capillary number, a certain fraction of collisions are below the critical offset and coalesce, while others exceed the critical offset and do not coalesce. The critical offset is therefore related to the so-called efficiency of coalescence [20], defined relative to the limit that neglects all direct (potential) and indirect (hydrodynamic) interactions [21]. Specifically, we define the volume-averaged coalescence efficiency [20],

$$\varepsilon_v = \frac{d\ln(a_v)}{dt}\frac{1}{\dot{\gamma}\phi_{\text{eff}}}\frac{\pi}{4(2-2^{2/3})}, \tag{3}$$

where ϕ_{eff} is the effective volume fraction of drops [19].

The experimental and theoretical coalescence efficiencies are essentially in accord when the drop viscosity is somewhat less than that of the continuous phase (e.g., $\hat{\eta} \approx 0.2$), the interface is clean, i.e., without surfactant, and the drops are not much larger than the size that leads to the onset of film drainage [5,19]. Direct experimental observation of film drainage [3], during head-on collisions in fluids with clean interfaces and $\hat{\eta} = 0.1$, agrees qualitatively, but not quantitatively, with theoretical analysis. These quantitative differences may arise in part from uncertainty in experimental measurement of the drainage time. Some unexpected results have been observed in recent experimental investigations, involving mixed flow type, of film drainage between drops that have somewhat higher viscosity than their surroundings [22]. Experiments with surfactant indicate that its effects seem to saturate when the amount of adsorbed surfactant is quite small [16,22]. These effects should be explored further.

In this paper, we report the orthokinetic coalescence efficiency (based on the evolution of the volume-averaged drop size) of fluid mixtures containing surfactant as a function of shear rate. By adjusting temperature, copolymer molecular mass, and concentration, we adjust the level of copolymer adsorption, the surface pressure, surfactant diffusion rates, and interfacial mobility. By this means we seek to determine the relevant parameters that govern shear-induced coalescence behavior, especially in mixtures with surfactant.

2. Materials and methods

The two fluids used in this study are poly(ethylene glycol) (PEG; the continuous phase; PolySciences), and poly(propylene glycol) (PPG; the droplet phase; Arco Chemical Co.).[1] Their number-average molecular weights are $M_n = 10{,}000$ and 12,200, respectively. The polydispersity of molecular weight for each is approximately $M_w/M_n = 1.1$, where M_w is the mass-averaged molecular weight, as determined by matrix-assisted laser-desorption-ionization (MALDI) mass spectroscopy. Their individual viscosities were measured using Carrimed and ARES cone-and-plate rheometers and found to be Newtonian up to shear rates of at least 800 s^{-1} (Table 2). The viscosity ratio $\hat{\eta}$ is approximately 0.2 at all temperatures. Because of the chemical similarity of PEG and PPG, σ is relatively small, and impurities are not likely to be surface-active. Nevertheless, the blend mixtures are strongly phase-separated; i.e., the solubility of one polymer in the other is negligible, because $10 \leqslant \chi N \leqslant 20$, where χ is the Flory interaction parameter and N is the effective degree of polymerization, defined below.

Table 2
Material viscosity

Material	T (°C)	η (Pa s)
PEG 10k	75	4.1
	90	2.7
	125	1.0
PPG 12.2k	75	0.71
	90	0.50
	125	0.2

Surface-active poly(ethyleneglycol-*b*-propyleneoxide-*b*-ethyleneglycol) ($EO_\alpha PO_\beta EO_\alpha$) triblock copolymers (Pluronic P85 ($EO_{26}PO_{40}EO_{26}$), P105 ($EO_{37}PO_{56}EO_{37}$), and F127 ($EO_{100}PO_{65}EO_{100}$), from BASF) were used as surfactants, and their adsorption onto the interface between PEG and PPG fluids was investigated. Pluronic P85 and P105 contain a mass fraction of PO $w_{\text{PO}} = 0.50$, while F127 contains only $w_{\text{PO}} = 0.30$. Their average molecular masses are 4800, 6500, and 12,600, respectively. Their polydispersity index (M_w/M_n) as specified by BASF is approximately 1.4 [23]. All polymers and copolymers are hydroxy-terminated.

The effective degree of polymerization of each polymer and chain segment is based on an equivalent monomer volume $\bar{v}$, given by the geometric mean,

$$\bar{v} = \sqrt{\text{Mo}_\text{A}\text{Mo}_\text{B}/(\rho_\text{A}\rho_\text{B})}/\mathcal{N}_\text{Av}, \tag{4}$$

where Mo_i is the molecular mass of monomer i, ρ_i is the mass density of homopolymer i, and $\mathcal{N}_\text{Av}$ is Avogadro's number. For mixtures of PO and EO, $\bar{v}$ is approximately 80.5, 81.4, and 83.3 Å^3, at 75, 90, and 125 °C, respectively. Based on this scaling, the degree of polymerization N (i.e., N_{hPEG} and N_{hPPG}) of the EO and PO homopolymers is approximately 191 and 260, respectively. (Since N_{hPEG} is significantly smaller than N_{hPPG}, each of the copolymer surfactants is much more soluble in the PEG continuous phase, and by comparison they are insoluble in the PPG drops. Therefore, the surfactants were added only to the PEG homopolymer.) Similarly, N for the copolymer surfactants is

[1] Certain commercial materials and equipment are identified in this paper in order to adequately specify the experimental procedure. In no case does such identification imply recommendation or endorsement by the National Institute of Standards and Technology, nor does it imply that these are necessarily the best available for the purpose.

93, 131, and 249, respectively. The volume fraction of PO in the copolymers $f(\mathrm{PO})$ is 0.53, 0.53, and 0.32.

To accomplish interfacial tension and coalescence efficiency measurements, mixtures were examined with monochromatic light by bright-field or phase-contrast optical microscopy using a Linkam Scientific Instruments CSS-450 heated shearing cell mounted on an Olympus microscope equipped with 10× and 20× long-working-distance objectives, various camera eyepieces, and a (640 × 480) pixel 8-bit CCD camera. The image magnification was determined using a calibrated ruling. The shear cell has a parallel-plate geometry, in which one quartz disk is rotated relative to another. The smaller disk has a radius of 15 mm, and the observation window is situated at a radius of 7.5 mm, so that the shear field is relatively uniform (i.e., ±3%) throughout the 0.52-mm-wide field of view. All shear rates and strains are reported at the location of the center of the window.

The interfacial tension between the two fluids was measured by the droplet retraction technique [24] as a function of temperature (75, 90, and 125 ± 0.1 °C) and copolymer concentration ($\phi_{\mathrm{bcp}} = 0$, 0.0025, 0.0050, and 0.0100 ± 0.0001). A very small amount of PPG ($\phi = 0.005$) was added to the PEG/copolymer mixture. Large (≈100-μm radius) isolated droplets were investigated by bright-field optical microscopy using a Linkam Scientific Instruments CSS-450 heated shearing cell having quartz windows in a parallel-plate geometry. The spacing h_{plate} between quartz plates was set to 500 μm. Ring tensiometry [25] was also performed on homopolymer blend interfaces, yielding similar results.

For drop retraction measurements, a 10× long-working-distance objective was used, and the image magnification (0.766 μm/pixel) was determined using a calibrated ruling. An impulse shear strain (100%) was applied and images of the subsequent relaxation of the droplet were acquired at intervals of typically 1/30 s. For each mixture, the response of four individual droplets was tested three times for each drop (see Fig. 1).

Coalescence experiments were carried out at gap spacings of 100 and 200 ± 4 μm, temperatures of 75, 90, and 125 ± 0.1 °C, disperse phase concentration $\phi = 0.055 \pm 0.0001$, and $\phi_{\mathrm{bcp}} = 0$, 0.0025, 0.0050, and 0.0100 ± 0.0001. The mixture was first sheared at high rate (e.g., 400 s^{-1}) to produce a relatively narrow distribution of small drops. Even at these rates, the Reynolds number $Re = \rho\dot{\gamma}h_{\mathrm{plate}}^2/\eta_c$ ($\rho \equiv$ density, $h_{\mathrm{plate}} \equiv$ gap spacing) is small ($\approx 3 \times 10^{-3}$), so that Stokes flow can be assumed. a_v produced by breakup was consistent within ±20% with the interfacial tension measured by retraction. For example, a 30% reduction in σ caused a roughly 30% reduction in steady-state drop size at the same shear rate. Therefore, the shear rate was adjusted slightly, so that for all temperatures and copolymer concentrations the starting drop size was more or less the same. After more than 1 min of preshear, the shear rate was decreased abruptly. In some instances, a secondary bulk flow was observed as drops drifted slightly transverse to the flow (along the vorticity axis) for a few seconds following the step down. When this drift occurred, the system was observed carefully to ensure that no significant coalescence took place during this time. Because the gap spacing is narrow, wall effects on the effective disperse phase volume fraction ϕ_{eff} (see Eq. (3)) are significant and are treated as described previously [19,45].

A series of images was recorded during shear at regular intervals of strain. The beginning of the series was timed such that the first one or two images were during rapid shear, so that the beginning of slow shear could be determined. The drop size distribution was measured from the images with an image analysis routine using the Danielson or circles operator, which fits a binary thresholded image with circular domains, as described previously [19]. During slow shear, Ca is small enough (<0.1) that the drops are nearly spherical. a_v was calculated as described previously [19]. The total number of drops counted per image is approximately 500 to 3000. Comparing the value of a_v resulting from different threshold values (e.g., 100 ⩽ gray-level ⩽ 120), the standard uncertainty in a_v is ±0.1 μm. Coalescence efficiency ε_v was measured at each time t_j according to Eq. (3), by a least-squares fit of $\ln(a_v)$ at times t_{j-2} through t_{j+2}, where j indexes sequential data points (for representative plots of $\log(a_v)$ vs dimensionless time, see Fig. 2). From the scatter of data points in Fig. 3, the measurement uncertainty in ε_v is approximately 20%.

3. Results and discussion

3.1. Sorption

The adsorption of copolymer onto the interface was evaluated by interfacial tension measurement via droplet retraction. The relaxation of a spheroidal droplet toward an equilibrium spherical shape is exponential [24,26],

$$\mathcal{D} = \mathcal{D}_0 \exp\{-t/\tau_d\}, \tag{5}$$

where $\mathcal{D}$ is the droplet deformation $= (L - B)/(L + B)$, defined by Taylor [27], where L is the major axis of the spheroid and B is its minor axis. τ_d is the drop shape relaxation time $\tau_d = \eta_{\mathrm{eff}} a_0/\sigma$, where a_0 is the radius of the undistorted sphere and η_{eff} is a viscosity parameter [26,27]

$$\eta_{\mathrm{eff}} = \left[\frac{(2\hat{\eta}+3)(19\hat{\eta}+16)}{40(\hat{\eta}+1)}\right]\eta_c.$$

Since the major axis is tilted out of the plane of the image, it is easier to measure the minor axis, B, and L is calculated assuming constant droplet volume $= 8a_0^3/B^2$. The projection of L was also measured, and the ratio of the measured value to the calculated value was constant after the first one or two data points. This behavior is consistent with an initially ellipsoidal shape, of which the two minor axes equilibrate substantially before the retraction of the major axis [28]. To normalize the data based on the drop size a_0 and the magnitude of the initial deformation $\mathcal{D}_0$, the data are plotted as

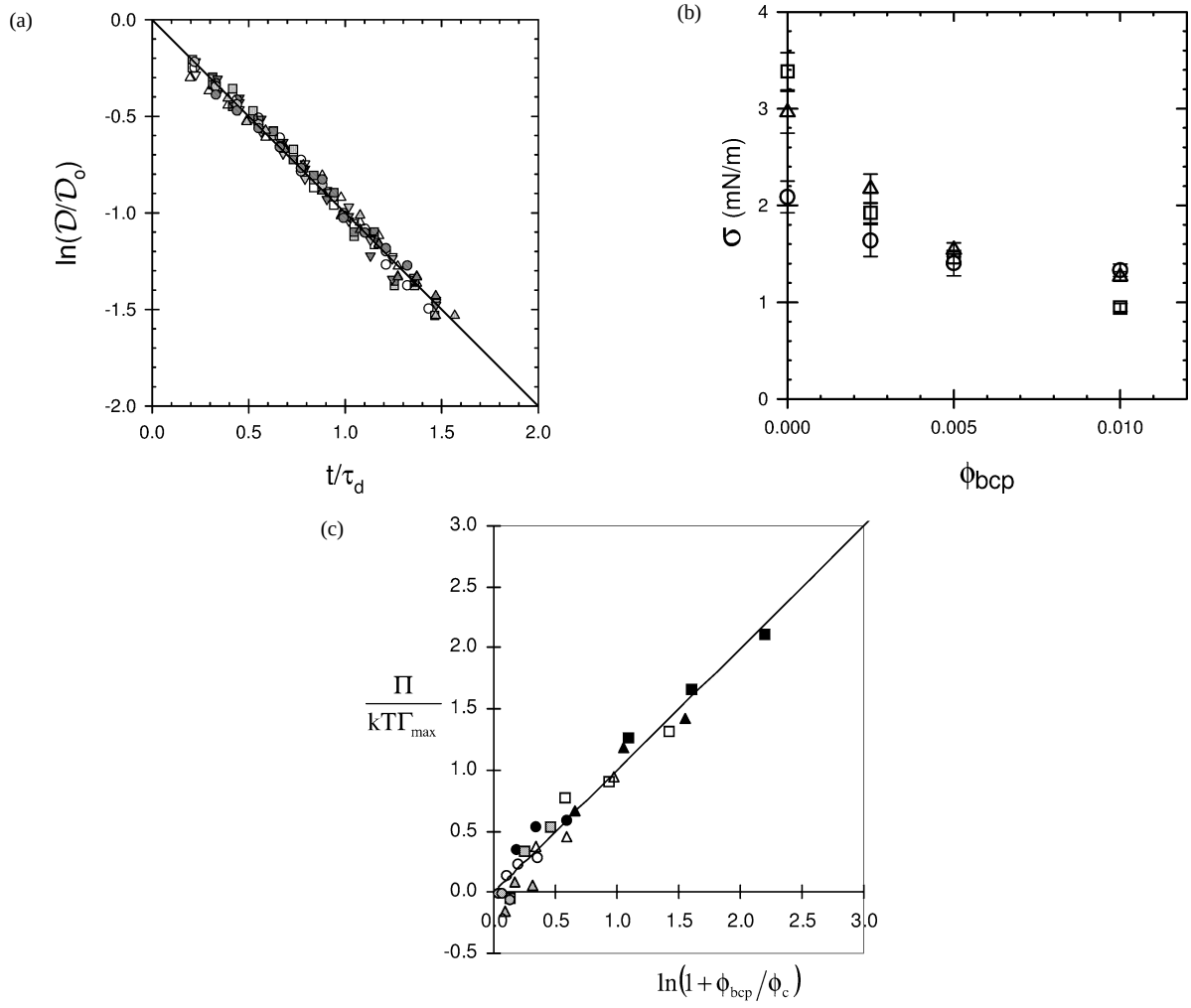

Fig. 1. Measurement of interfacial tension by droplet retraction. (a) Rescaled deformation vs time, shown here for $\phi_{\mathrm{bcp}}(\mathrm{F127}) = 0.0100$ at 75 °C. Different symbols (circles, triangles, upside-down triangles, and squares, respectively) represent data from different drops, whose undistorted diameters were 198, 203, 214, and 228 μm. See text for details of rescaling. The line represents a least-squares fit. (b) Interfacial tension of PEG and PPG, as a function of ϕ_{bcp}(F127) and of temperature (squares, triangles, and circles represent data at 75, 90, and 125 °C, respectively). Error bars represent the values of σ that cause a doubling of the sum of square errors. The measurement uncertainty determined in this way ranges from 4 to 10%. (c) Dimensionless surface pressure vs $\ln(1+\phi_{\mathrm{bcp}}/\phi_c)$; see Eq. (10). As with the previous figure, squares, triangles, and circles represent data at 75, 90, and 125 °C, respectively. Shaded, open, and filled symbols represent data of P85, P105, and F127, respectively. See the text for details of the analysis.

$\ln(\mathcal{D}/\mathcal{D}_0)$ versus t/τ_d (Fig. 1). A single value of σ and individual values of $\mathcal{D}_0$ are adjusted to provide a best fit to Eq. (5). For each mixture, the data set is more or less self-consistent and the relaxation follows an essentially single exponential (Fig. 1).

In mixtures containing copolymer, the interfacial tension is reduced from that of the binary homopolymer mixture (Fig. 1b). Whereas the interfacial tension without copolymer decreases with increasing temperature, the effect of temperature is qualitatively different at high surfactant concentrations, and increasing temperature increases the interfacial tension. These results indicate that higher temperature causes the copolymer to be more soluble, so that less is adsorbed to the interface.

The difference in surface tension with and without copolymer, i.e., the surface pressure Π, was measured for the three copolymers as a function of temperature and concentration. The Langmuir model assumes that sorption obeys first-order reaction rates,

$$d\Gamma/dt = k_a\phi_s(\Gamma_{\max} - \Gamma) - k_d\Gamma, \tag{6}$$

where ϕ_s is the concentration of copolymer dissolved in the layer of bulk fluid adjacent to the interface (expressed as a volume fraction). k_a and k_d are rate constants for adsorption and desorption, respectively. Solving Eq. (6) at equilibrium (zero net rate $d\Gamma/dt = 0$ and zero concentration gradients $\phi_s = \phi_{\mathrm{bcp}}$), the adsorption isotherm becomes

$$\frac{\Gamma}{\Gamma_{\max}} = \frac{\phi_{\mathrm{bcp}}/\phi_c}{1 + \phi_{\mathrm{bcp}}/\phi_c}, \tag{7}$$

where ϕ_{bcp} is the volume fraction of copolymer dissolved in the bulk, $\Gamma_{\max}$ is the maximum interfacial concentration

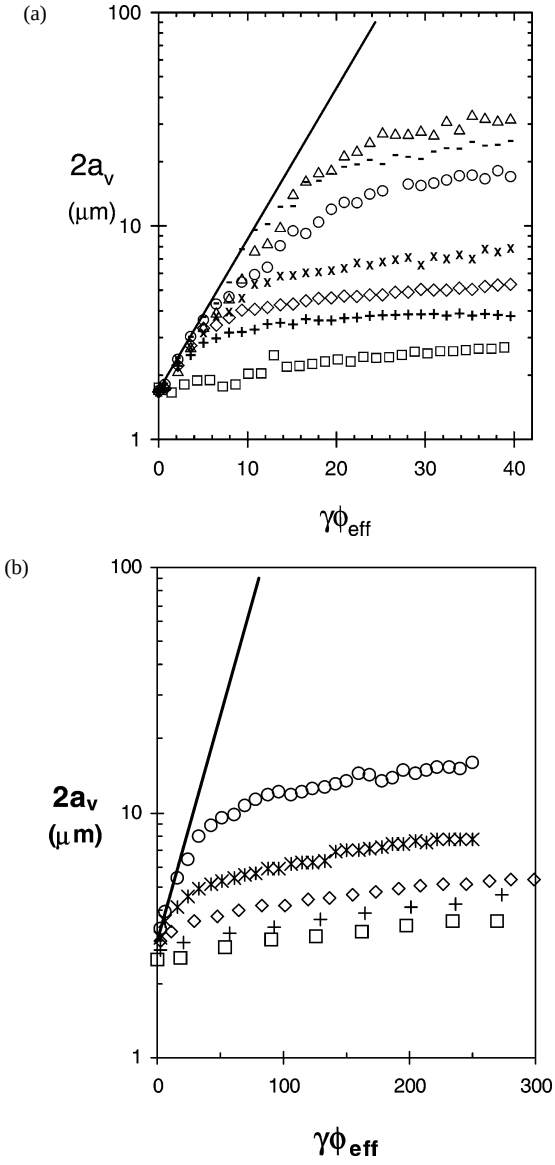

Fig. 2. Drop size vs dimensionless time, where ϕ_{eff} is defined previously [19]. (a) $\phi_{\text{bcp}}(\text{P85}) = 0.0100$; $T = 75\,^{\circ}\text{C}$. (b) $\phi_{\text{bcp}}(\text{F127}) = 0.0005$; $T = 75\,^{\circ}\text{C}$. The symbols represent shear rates, 0.5 s^{-1} (triangle), 1 s^{-1} (−), 2 s^{-1} (circle), 5 s^{-1} (×), 10 s^{-1} (diamond), 20 s^{-1} (+), and 50 s^{-1} (square). The dispersed phase concentration for each mixture was $\phi = 0.055$.

of copolymer, and $1/\phi_c$ is the equilibrium constant (i.e., the nondimensional ratio of adsorption and desorption rate constants $K = 1/\phi_c = k_a/k_d$). Other models of adsorption yield similar adsorption isotherms (e.g., [29,30]).

$\Gamma_{\max}$ may be approximated as

$$\Gamma_{\max} = \frac{d}{v_{\text{bcp}}} = \frac{\bar{v}^{1/3}(N/n)^{1/2}}{\bar{v}N}, \tag{8}$$

where the numerator represents the thickness d of a dense interfacial copolymer layer and the denominator is the molecular volume v_{bcp}. N is the effective total degree of polymerization of the surfactant. $n = 1$ for a diblock copolymer and 2 for a triblock copolymer (i.e., in the loop conformation). For the three copolymers studied, the calculated $\Gamma_{\max}$ equals approximately 0.39, 0.33, and 0.24 nm^{-2}, with increasing molecular mass. The equilibrium constant may be expressed in terms of an approximation of activation energy for desorption,

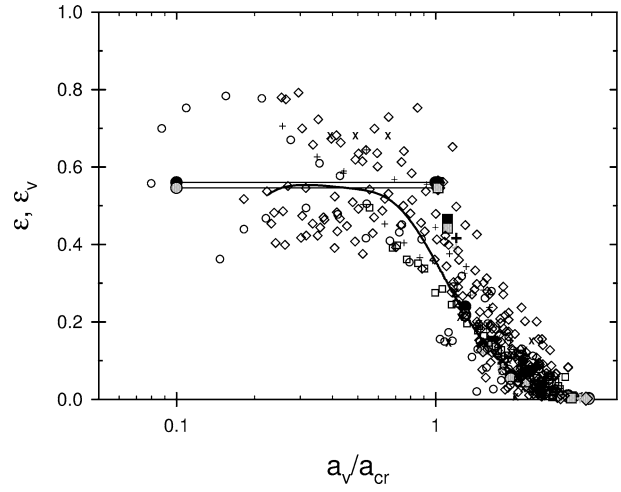

Fig. 3. Coalescence efficiency ε_v vs a_v/a_{cr}, for binary mixtures of PPG drops in PEG at 90 °C. The open symbols represent experimental data ε_v [19]. Several experiments are reported in which $\phi = 0.022$, 0.044, 0.055, and 0.110, and gap spacing = 50, 100, and 200 μm. Shear rates are represented by different symbols, i.e., 2 s^{-1} (circle), 5 s^{-1} (×), 10 s^{-1} (diamond), 20 s^{-1} (+), and 50 s^{-1} (square). Filled and shaded symbols represent calculations based on individual drop pairs, whose size ratio is 1 and 0.75, respectively. The curve corresponds to ε_v predicted at 2 s^{-1}. Consult the text for additional details.

$$K = 1/\phi_c = \exp(\Delta G/k_{\text{B}}T) = \exp(\chi N f_{\text{PO}}), \tag{9}$$

where k_{B} is Boltzmann's constant, χ is the segmental interaction parameter between EO and PO, and Nf_{PO} is the length of the PO block in the copolymer, which adsorbs from solution to the interface [31].

Applying the Gibbs equation, the interfacial tension is

$$\sigma = \sigma_0 + k_{\text{B}}T\Gamma_{\max}\ln(1 - \Gamma/\Gamma_{\max}),$$
$$\sigma = \sigma_0 - k_{\text{B}}T\Gamma_{\max}\ln(1 + \phi_{\text{bcp}}/\phi_c). \tag{10}$$

The Flory interaction parameter between EO and PO segments determined by a least-squares fit to the data (Fig. 1c) is $\chi = A/T + B = 81/T - 0.15$, in reasonable agreement with the previously reported values [32,33], after accounting for different definitions of $\bar{v}$ (cf. Eq. (4)).

The results of adsorption measurements and associated model parameters ϕ_c, Π, σ_0, $\Gamma_{\max}$, v_{bcp}, and k_d are used to evaluate various parameters discussed in the following sections. In the following experiments to measure the coalescence efficiency, the relative interfacial concentration $\Gamma/\Gamma_{\max}$ ranged from 0.03 to 0.37 for mixtures containing P85 and from 0.04 to 0.67 for mixtures containing F127.

3.2. Coalescence in mixtures without surfactants

To begin, we replot data (a_v vs dimensionless time) reported previously [19], here as efficiency ε_v vs a_v/a_{cr}

(Fig. 3; see Eqs. (1) and (3)). As discussed before [19], experimental and theoretical results are roughly consistent, with each having a constant $\varepsilon_v \approx 0.56$ at small Ca (no adjustable parameters) and an arrest of coalescence that begins approximately when $a_v > a_{cr}$ (the Hamaker parameter having been adjusted to 10^{-19} J). Theoretical results are based on calculated drop trajectories, using an asymptotic analysis of drop trajectories and film drainage [6]. The individual pair coalescence efficiencies were determined for each of five shear rates (2, 5, 10, 20, and 50 s^{-1}), five drop size ratios (0.1, 0.3, 0.5, 0.75, and 1) and six drop sizes, the critical drop radius and five larger values (Fig. 3, filled symbols). The efficiencies of other collisions (of different drop size or size ratio) were calculated by interpolation. From these individual pair efficiencies, the evolution of drop size distributions was calculated. Based on the growth of the volume-averaged drop size, a coalescence efficiency ε_v was calculated (Fig. 3, curve), thereby making the connection from individual drop trajectories to the dynamics of large populations. At small values of a_v/a_{cr}, the critical offset is defined only by the drop trajectory; deformation and film drainage are unimportant, so that the coalescence efficiency is constant and matches the prediction that assumes spherical drops. When $a_v \approx a_{cr}$, ε_v begins to decrease. As Ca and a_v/a_{cr} increase, a smaller fraction of collisions results in coalescence. The efficiency becomes very small indeed, as the critical offset approaches that which produces nearly a head-on collision. At large values of a_v/a_{cr}, coalescence is essentially arrested. Evidently (Fig. 3), the effect of polydispersity smoothes the transition from spherical drop behavior ($a_v/a_{cr} < 1$) to that of deformed drops ($a_v/a_{cr} > 1$).

3.3. Coalescence in mixtures with surfactants

Next, we explore the effect of surfactant. a_v grows with time in a manner qualitatively similar to that observed in mixtures without surfactant [19]: the growth rate is rapid at small Ca, and the rate decreases dramatically at larger Ca (Fig. 2). As with surfactant-free mixtures, the coalescence efficiency reduces to a similar curve when plotted against a_v/a_{cr} (Fig. 4), using parameters (such as interfacial tension) appropriate for the mixture containing surfactant. That is, ε_v is constant at low Ca, and then plummets at larger Ca, as coalescence is arrested. However, the presence of surfactant introduces two effects: (1) the limiting coalescence efficiency at very small Ca is diminished, and (2) the arrest of coalescence occurs at smaller Ca (the critical value of a_v/a_{cr} is no longer 1, but severalfold less). Although the data at different shear rates are well superposed by plotting ε_v against a_v/a_{cr}, the limiting coalescence efficiency at low Ca and the critical value of a_v/a_{cr} depend on temperature, surfactant concentration, and surfactant molecular weight (Figs. 4 and 5), suggesting the existence of a more appropriate governing parameter, to be discussed later. At higher molecular weight, lower temperature, or higher ϕ_{bcp}, as the adsorption of copolymer becomes stronger, the limiting value of

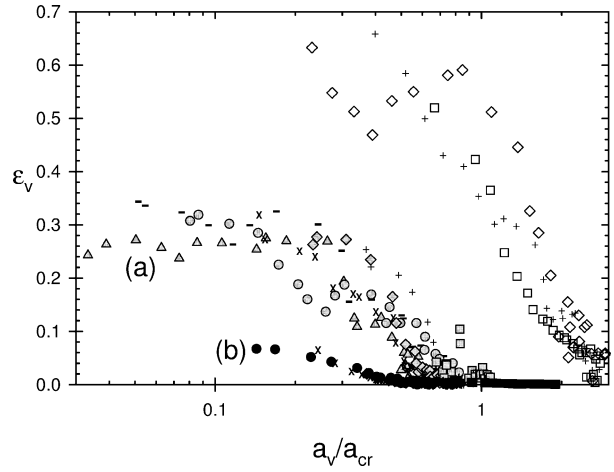

Fig. 4. Coalescence efficiencies derived from the data sets in Fig. 2 are plotted vs a_v/a_{cr}: (a) (ϕ_{bcp}(P85) = 0.0100, shown here with shaded symbols) and (b) (ϕ_{bcp}(F127) = 0.0005, filled symbols). Shear rates are indicated as in previous figures. Coalescence efficiency data from a surfactant-free mixture also at 75 °C are also shown (open symbols). The Hamaker parameter was assumed to be independent of temperature. Note while the interfacial tension reduction is modest, i.e., $(\sigma_0 - \sigma)/\sigma_0$ equals (a) 0.29 and (b) 0.11, the coalescence efficiency is reduced dramatically. Indeed, the more substantial effect here is exhibited at the higher surface tension (b). As discussed in the text, the interfacial tension gradient is limited by diffusion of surfactant in the bulk phase, to and from the interface, which is significantly slower, when the surfactant molecular weight is higher and its concentration is lower (as for data set (b)).

ε_v at low Ca and the critical value of a_v/a_{cr} for the onset of the arrest of coalescence both decrease. However, the effect of molecular weight reaches saturation, as indicated by reasonable superposition of the data from systems containing higher molecular weight copolymer (Fig. 5b).

Clearly, these effects must be attributed to a change in interfacial properties, associated with the presence of surfactant. However, there are a number of questions concerning the nature of these phenomena. At the critical condition for the onset of arrest of coalescence, the deformation of the drops (as measured by b/a_{cr}) is much less when surfactant is present—often more than an order of magnitude less. Perhaps then the drops are essentially spherical, and the arrest of coalescence is not associated with the onset of deformation? Rather it may be associated with the effects of drop size on surfactant mass transfer, so that the interface becomes immobile when the drop exceeds a certain size. If so, is the mobility reduced over the entire drop surface, or just in an isolated region? Does surfactant immobilize the interface, or merely reduce its mobility? What are the dominant mechanisms of surfactant transport? Is arrest of coalescence associated with a change in the dominant transport mechanism? Is surfactant sorption important, or does the surfactant behave as insoluble on the drop collision time scale? What, if any, is the role of drop deformation? We address these questions, and the issues of drop deformation and surfactant mass transfer, through the following analysis, which involves the use of several Peclet numbers, defined in Table 1.

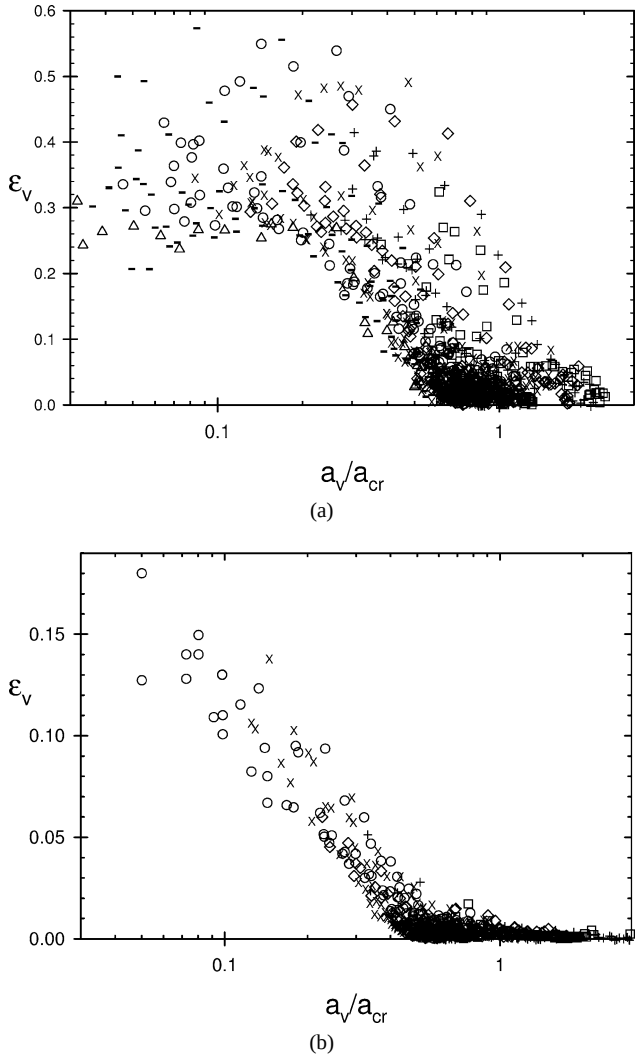

Fig. 5. Compilations, ε_v vs a_v/a_{cr}, of six data sets for each surfactant. Each mixture was tested at temperatures 75, 90, and 125 °C. Shear rates are indicated as in previous figures. The dispersed phase concentration for each mixture was $\phi = 0.055$. (a) Mixtures containing P85 surfactant, $\phi_{\mathrm{bcp}} = 0.0025$ and 0.0100. Note that the critical value of a_v/a_{cr} ranges from approximately 0.2 to 0.5 (as the strength of adsorption decreases). (b) Mixtures containing F127 surfactant, $\phi_{\mathrm{bcp}} = 0.0005$ and 0.0025, for which the critical value of $a_v/a_{\mathrm{cr}} < 0.1$.

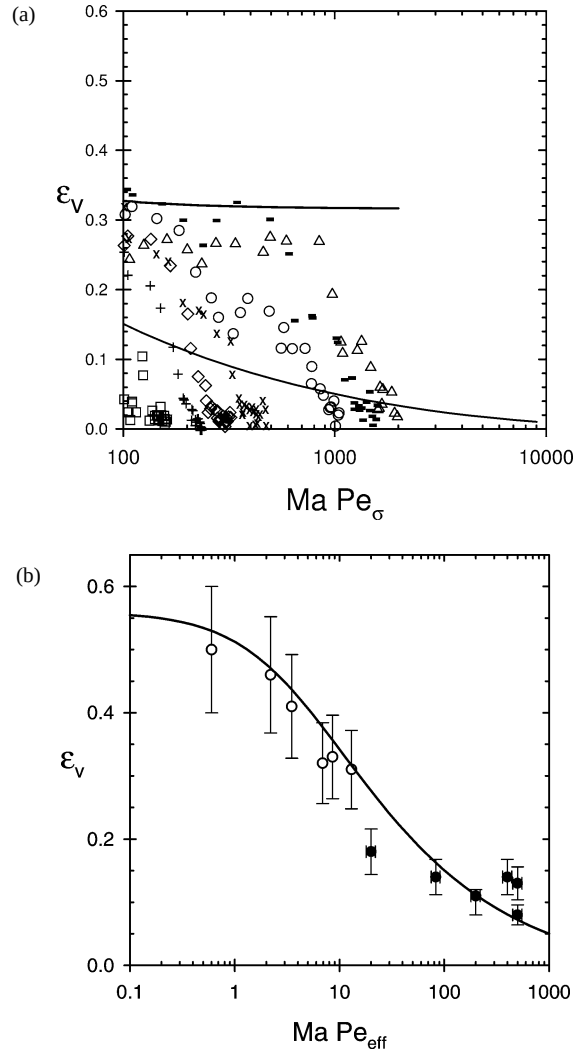

Fig. 6. (a) The data of Fig. 4a plotted against $Ma\,Pe_\sigma$. The lower curve is the prediction of Blawzdziewicz et al. [9], assuming insoluble surfactant. The upper curve is the prediction obtained from an *ad hoc* modification to this theory [9], using an effective Peclet number that accounts for sorption, as discussed in the text (Eq. (14)). (b) The coalescence efficiency vs $Ma\,Pe_{\mathrm{eff}}$, using the *ad hoc* substitution of Eq. (14) into Eqs. (12), represented by the curve. The symbols denote measurements of ε_v at small Ca.

3.4. The effect of surfactants on drop trajectory

3.4.1. Insoluble surfactants

If the surfactant retards the motion of the interface, the trajectory of the drop is deflected more and the coalescence efficiency decreases [9], in a manner qualitatively analogous to the effect of increasing drop viscosity. Assuming the surfactant is insoluble, the parameter that gauges the mobility of the interface is $Ma\,Pe_\sigma$, as discussed in Section 1 (Eq. (2)) [12]. For drop trajectory phenomena, the relevant length scale is the drop radius a_v, so that $Pe_\sigma = \dot{\gamma} a_v^2/D_\sigma$ (Table 1). To estimate the surface diffusion coefficient D_σ, we assume that the interfacial diffusivity of copolymer surfactant is equal to the bulk diffusivity D of equivalent molecular weight PEG in the melt state, which has been reported in the literature [34]. Actually, the diffusion coefficient of *microsegregated* block copolymers is somewhat less (few- to several-fold) than in an ideal disordered melt [35]. The approximation is likely to be worst for F127, since increasing molecular weight amplifies the effects of microsegregation and chain entanglement [35]. Such errors in estimation of D_σ are not large enough to significantly influence the major conclusions of this paper. Using this approximation, coalescence efficiency is plotted against $Ma\,Pe_\sigma$ in Fig. 6. Clearly this analysis fails to superpose the data.

Computing $Ma\,Pe_\sigma$, we find:

$$Ma\,Pe_\sigma = \frac{\Pi}{\sigma_0 \mathrm{Ca}} \frac{\dot{\gamma} a_v^2}{D_\sigma} = \frac{\Pi \sigma}{\sigma_0 \eta_c} \frac{a_v}{D_\sigma} \sim \dot{\gamma}^0 a_v^1. \tag{11}$$

Note that this parameter scales with a_v, indicating that the interface mobility decreases with increasing drop size, a trend that is consistent with the arrest of coalescence at large a_v. However, proceeding with the analysis, we find a number of significant discrepancies with the experimental results.

Blawzdziewicz et al. [9] have calculated the coalescence efficiency ε of equal-sized drops as a function of $Ma\,Pe_\sigma$ in the limit of Ma being large compared to a_v/h, where h is the separation between drops. The following expression (Eq. (5.17) in their paper [9]) approximates their results,

$$\varepsilon \approx 1.0409\left(\Lambda^{0.20892} - (1.9269\times 10^{-5})^{0.20892}\right)^{3/2}, \quad (12a)$$

where, if we include the effect of drop viscosity [36],

$$\Lambda = 1\big/\left(3(1+\hat{\eta}) + Ma\,Pe_\sigma\right). \quad (12b)$$

Equations (12) predict a gradual decrease in ε as $Ma\,Pe_\sigma$ increases (Fig. 6). In contrast, experimentally, the arrest of coalescence is much more abrupt. Moreover, Eqs. (11) and (12) do not predict the observed constant coalescence efficiency at small Ca. Experimentally, Ma here ranges typically between 1 and 100, and it exceeds 100 for more than 10 data points shown in Fig. 6a, at smallest Ca. Since these values of Ma are not exceedingly large, we are not concerned with quantitative, but qualitative comparison with this theory [9]. Qualitative comparisons are useful, because even for modest values of Ma, the relevant parameter for insoluble surfactant is $Ma\,Pe_\sigma$ (Eq. (2)). We maintain this perspective throughout the paper, by dimensional analysis seeking to determine the appropriate governing parameters, and not focusing on quantitative comparison with theories, because we anticipate future theoretical development.

Milner and Xi also calculated surfactant-induced adjustments to drop trajectories and their consequences for coalescence efficiency [37]. They considered Pe_σ to be infinite, so that the copolymer concentration gradient on the surface of the drop produced during collision is determined by considering the copolymers as merely markers on the drop surface. The concentration gradient is therefore independent of the shear rate. By perturbation analysis, the effect of copolymer on the approach of two droplets is proportional to the energy expended to produce this concentration gradient, relative to the hydrodynamic energy dissipated during collision. In other words, the effect of copolymer is proportional to the Marangoni number, which becomes the controlling parameter here. While the work of compressing the surfactant layer is independent of shear rate, the hydrodynamic dissipation is proportional to it. Indeed, rewriting Milner and Xi's equation (16) (or (18)) yields the following dimensionless force coefficient [37]

$$f = \frac{16}{5}\frac{\Pi}{\sigma \mathrm{Ca}} = \frac{16}{5}\frac{\sigma_0}{\sigma}Ma \sim a_v^{-1}\dot{\gamma}^{-1}. \quad (13)$$

Since ε decreases as f increases, this theory predicts that the smallest coalescence efficiency occurs at the smallest shear rate and drop size, where the hydrodynamic dissipation is small. This scaling prediction is in complete opposition to our experimental observations. Finally, since the Marangoni number in our experiments is often substantially larger than unity, the coalescence efficiency predicted from their model is essentially zero.

In summary, the insoluble surfactant trajectory concept fails to describe our experimental results: specifically, (1) the parameter $Ma\,Pe_\sigma$ fails to superpose the data (Fig. 6a), and (2) theories based on this concept differ qualitatively from experimental observations. The failure of the insoluble-copolymer/drop-trajectory concept suggests the importance of sorption phenomena and/or deformation and film drainage. We turn first to the effects of sorption.

3.4.2. Soluble surfactants

Whereas with insoluble surfactants, interfacial concentration gradients dissipate only by surface diffusion, sorption of copolymer to and from the interface can simultaneously reduce such gradients. Whichever is faster, sorption or interfacial diffusion, is the dominant mechanism to reduce interfacial concentration gradients. Sorption itself involves two processes, bulk diffusion and local kinetic equilibration at the interface; their being in series dictates that sorption is limited by the slower of these two. Thus, surfactant mass transport and the dissipation of interfacial concentration gradients may be dominated by any of the three processes. Specifically, interfacial concentration gradients are proportional to (a) the surface Peclet number (Pe_σ), (b) the product of the bulk Peclet number and the dimensionless diffusion depth (HPe), or (c) the ratio of shear rate to the kinetic rate constant for desorption ($\dot{\gamma}/k_d$), i.e., the Biot number, depending on whether the surfactant mass transfer is dominated by surface diffusion, bulk diffusion, or interfacial kinetics, respectively. Holbrook and Levan [14,15] evaluated ratios of these numbers to determine the dominant mass transfer process. To account for the parallel and serial processes simultaneously, we propose the following dimensionless group:

$$Pe_{\mathrm{eff}} = \frac{Pe_\sigma(HPe + \dot{\gamma}/k_d)}{Pe_\sigma + HPe + \dot{\gamma}/k_d}. \quad (14)$$

Before this parameter is evaluated, it is necessary to compute its constituents. Since the relevant length scale remains the drop radius, the bulk Peclet number is $Pe = \dot{\gamma}a_v^2/D$, where D is the diffusivity of the copolymer in solution with the PEG homopolymer, which we again approximate as the diffusivity of equivalent molecular weight PEG. The kinetic adsorption coefficient k_a may be estimated from the time for a copolymer to diffuse to the interface from an immediately adjacent region, i.e., to diffuse a distance equal to the thickness of the interfacial copolymer layer, d. Thus, $k_a \sim D/d^2$. Somewhat slower kinetics are expected if there is an activation energy for adsorption. The kinetic rate constant for desorption is obtained from the definition $k_d = k_a\phi_c$.

The effective dimensionless diffusion depth noted above is written

$$H = \frac{\Gamma_{\max} v_{\mathrm{bcp}}}{(\phi_c + \phi_{\mathrm{bcp}}) a_v} \hat{z}, \tag{15}$$

where the first group is the dimensionless diffusion depth at small to moderate *Pe*, for which diffusion is undisturbed by convection and $\hat{z} \approx 1$. When *Pe* is very large, the diffusion layer becomes modified by convection, and $\hat{z} \sim Pe^{-1/2}$. We assume that $\hat{z} = 1$. Based on these estimates, the ratio

$$HPe \frac{k_d}{\dot{\gamma}} \approx \frac{\phi_c a_v}{(\phi_c + \phi_{\mathrm{bcp}}) d}$$

is greater than unity in all of our experiments, indicating that interface kinetics are much faster than bulk diffusion, so that sorption is diffusion-limited.

The relative importance of diffusion-limited sorption versus surface diffusion is evaluated by the ratio HPe/Pe_σ. According to the estimates described above, this number is less than unity, for most of our experiments, indicating that sorption by bulk diffusion occurs more rapidly than surface diffusion. Thus, concentration gradients are controlled by (diffusion-limited) sorption, and $Pe_{\mathrm{eff}} = HPe$. In this limit,

$$Ma\,Pe_{\mathrm{eff}} \approx Ma\,HPe \approx \frac{\Pi}{\sigma_0 \mathrm{Ca}} \frac{\Gamma_{\max} v_{\mathrm{bcp}}}{(\phi_c + \phi_{\mathrm{bcp}}) a_v} \frac{\dot{\gamma} a_v^2}{D} = \frac{\Pi \sigma}{\sigma_0 \eta_c} \frac{\Gamma_{\max} v_{\mathrm{bcp}}}{(\phi_c + \phi_{\mathrm{bcp}}) D} \sim \dot{\gamma}^0 a_v^0. \tag{16}$$

Note that this expression predicts that the interfacial mobility is *independent of shear rate and drop size*, in agreement with the experimental phenomenon at small Ca. This suggests that the reduction in coalescence efficiency at small Ca derives from bulk-diffusion-limited sorption, which retards the interface and thereby causes deviations in the drop trajectories, so that some collisions are avoided. Making the *ad hoc* assumption that $Ma\,Pe_{\mathrm{eff}}$ (Eq. (14)) can substituted for $Ma\,Pe_\sigma$ in Blawzdziewicz and Loewenberg's theory [9], Eq. (12) can be replotted (Fig. 6). Reasonable quantitative agreement with the data at low Ca (see Fig. 6b) is fortuitous, considering the various approximations involved. At large $Ma\,Pe_{\mathrm{eff}}$, the observed unexpectedly large values of ε_v (Fig. 6b) may arise from an underestimation of ϕ_{eff}. ϕ_{eff} is not expected to remain constant (as assumed in this analysis); instead, it is expected to increase at large $Ma\,Pe_{\mathrm{eff}}$, when the shear-induced drop diffusivity is reduced [45].

If sorption were limited by interfacial kinetics, then the relative importance of sorption and surface diffusion would be parameterized by

$$\frac{\dot{\gamma}}{k_d Pe_\sigma}$$

and

$$Ma\,Pe_{\mathrm{eff}} = Ma\dot{\gamma}/k_d = \frac{\Pi \sigma}{\sigma_0 \alpha \eta_c a_v} \sim \dot{\gamma}^0 a_v^{-1},$$

which is inconsistent with the data at small Ca. Note that regardless of whether the limiting surfactant mass transfer mechanism is interface diffusion, bulk diffusion, or interface kinetics, $Ma\,Pe_{\mathrm{eff}}$ and the concomitant ε_v are *independent of shear rate*. Dependence on shear rate is expected only in the limit of infinite Pe_{eff} [37,38].

3.5. The effect of surfactants on film drainage

Considering the whole drop, it appears that, for interfacial concentration gradients associated with that length scale, sorption is significant and that it is limited by bulk diffusion. When diffusion-limited sorption dominates, we suggest that the relevant parameter characterizing interfacial mobility, and therefore coalescence efficiency, is independent of shear rate and drop size, consistent with the data at low Ca.

At higher Ca, where the coalescence is being arrested, none of the parameters that arise from consideration of the whole drop are able to superpose the data. Thus, we infer that drop deformation during collision must be important in the arrest of coalescence, and we now consider the role of thin film drainage.

At the much smaller scale associated with the flattened film radius $b = (a_v \mathrm{Ca}^{1/2})$, Peclet numbers are correspondingly smaller (and H correspondingly larger), so that surface diffusion may become the dominant mechanism of surfactant mass transport (Eq. (14)), i.e., the surfactant may behave as insoluble. Furthermore (recalling that the copolymer is insoluble in the droplet phase), sorption is prevented by depletion of copolymer from the continuous-phase film, if the diffusion depth is more than half the film thickness h, i.e., when

$$h < h_{\mathrm{sorp}} = \frac{2\Gamma_{\max} v_{\mathrm{bcp}}}{(\phi_c + \phi_{\mathrm{bcp}})}.$$

Experimentally, the calculated value of h_{sorp} ranges from a minimum value of 80 nm ($\phi_{\mathrm{bcp}}(\mathrm{P85}) = 0.01$; $T = 125\,^\circ\mathrm{C}$) to a maximum of 6 μm ($\phi_{\mathrm{bcp}}(\mathrm{F127}) = 0.0005$; $T = 75\,^\circ\mathrm{C}$). Even the minimum value of h_{sorp} is larger than the critical film thickness h_c (which is expected to be between 10 and 20 nm [39]), so that in all cases, at the final stages of film drainage, surface diffusion is expected to be the dominant mechanism of surfactant mass transport. Thus, while the interfacial concentration gradients across the whole drop may be weak and controlled by sorption, more significant gradients may appear when the drops begin to deform in the near contact region, where surfactant sorption is irrelevant. Consequently, Marangoni stresses would only be substantial during the film drainage process.

The relevant Peclet number for film drainage with insoluble surfactant is $Pe'_{\sigma f} = v' b / D_\sigma$, where v' is the interfacial velocity, whose characteristic magnitude, according to Chesters and Bazhlekov, is $\sigma_0 b^2/(\eta_d a_v^2) = \sigma_0 \mathrm{Ca}/\eta_d$ [10]. The surface Peclet number in the film becomes

$$Pe_{\sigma f} = \sigma_0 a_v \mathrm{Ca}^{3/2}/(\eta_d D_\sigma). \tag{17}$$

While the corresponding relevant parameter for interfacial retardation is $Ma\,Pe_{\sigma f}$, it is important to consider the specific effects of interfacial mobility on the film drainage process.

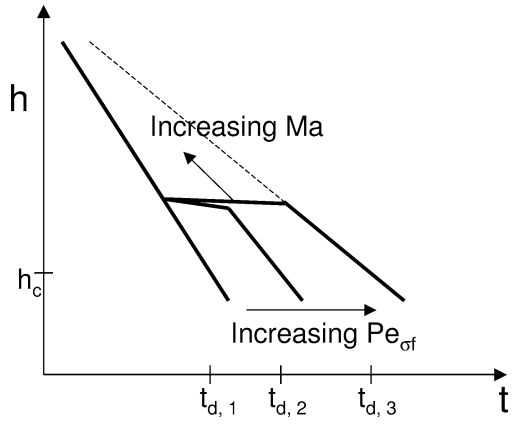

Fig. 7. Schematic log–log representation of film thickness h as a function of time t, adapted from Chesters and Bazhlekov [10]. The nearly horizontal lines at center represent the transitional pause described in the text. These shift to larger h as *Ma* increases. Curves at zero, intermediate, and infinite $Pe_{\sigma f}$ are sketched. Marked are corresponding drainage times to reach the critical film thickness h_c. The dashed line is the limit of continuously immobile interfaces.

The most detailed theoretical calculations of film drainage are by Chesters and Bazhlekov [10], who accounted for viscosity ratio and the presence of (insoluble) surfactant. Film drainage phenomena were shown to depend on four parameters: $\hat{\eta}$, *Ma* (which they write as Γ^*), $Pe_{\sigma f}$, and the dimensionless Hamaker parameter [7], which, as noted before, is related to $a_v/a_{\rm cr}$.

When *Ma* and $Pe_{\sigma f}$ are large enough and h_c is small enough (i.e., $a_{\rm cr}$ is small enough), the film surfaces become *immobile*, so that the drainage is very slow. The film drainage process is complex and roughly comprises three stages: mobile drainage, a transitional pause, and immobile drainage (Fig. 7) [10]. In the first stage, film drainage occurs at a rate that is nearly equal to the surfactant-free behavior. When the film reaches a certain thickness, the transitional pause takes place. At this stage, concentration gradients and attendant Marangoni stresses have become large enough, particularly at the rim of the film, so that the interfacial velocity there, for a time, is negative, and the center of the film swells slightly in thickness. During this period, the thickness of the film at the rim does not change much. Eventually, in the third stage, the interface velocity of the whole film is zero and the film continues to drain until it reaches h_c and the film ruptures.

The length of the transitional pause depends on $Pe_{\sigma f}$ and its timing depends on *Ma* [10]. In the limit of infinite $Pe_{\sigma f}$, the pause is maximum and the film thickness after the pause is essentially equal to that if fully immobile boundary conditions had been maintained from the beginning. Whether the pause occurs early (large *Ma*) or late (small *Ma*), eventually the same asymptote is reached. Thus, as long as the transitional pause occurs, *its timing is largely irrelevant*. However, if *Ma* is too small, the transitional pause will not occur before h reaches h_c, and mobile interface behavior will be observed. To delay film drainage, *Ma* needs to exceed a certain value, so that the pause occurs before film rupture. Since *Ma* depends on the amount of copolymer adsorbed to the interface, the effect of copolymer on film drainage is expected to saturate once there is sufficient copolymer to induce the transitional pause before film rupture. Further increase in the amount of copolymer, only serves to make the transitional pause occur earlier, and does not influence the film drainage time, and thus does not further reduce coalescence efficiency. At intermediate values of $Pe_{\sigma f}$, the pause is not so long, so that the film drainage time is intermediate between the mobile and immobile limits. While long after the transitional pause, the film drainage behavior seems to be insensitive to *Ma*, at somewhat shorter times after the pause, there seems to be some interplay between *Ma* and $Pe_{\sigma f}$ [10].

To account for the effects of *Ma* and $Pe_{\sigma f}$, we propose the parameter $Ma_{\rm eff}\,Pe_{\sigma f}$, where $Ma_{\rm eff}$ is defined as

$$Ma_{\rm eff} = Ma/(Ma_c + Ma), \tag{18}$$

so that for $Ma > Ma_c$, the transitional pause occurs early in the film drainage process and the effect of surfactant saturates. Choosing $Ma_c = 1$, the arrest of coalescence is rather well characterized by $Ma_{\rm eff}\,Pe_{\sigma f}$ (Fig. 8), in comparison to $a_v/a_{\rm cr}$ (Fig. 5), especially at small values of ε_v. The arrest begins when $Ma_{\rm eff}\,Pe_{\sigma f}$ is somewhat larger than 1 and the coalescence efficiency reaches near zero at values slightly larger than 100. The previous scaling (Fig. 5) does not consider Marangoni effects, and thus, unlike $Ma_{\rm eff}\,Pe_{\sigma f}$, it fails to superpose data obtained at weak *Ma* with those obtained at strong *Ma*. When *Ma* is large, however, $Ma_{\rm eff}$ is constant (because Marangoni forces are large enough to induce the transitional pause sufficiently early). Therefore, at large *Ma*, $a_v/a_{\rm cr}$ ($\sim\dot{\gamma}^{2/3}a_v$) and $a_v/a_{{\rm cr},s}$ ($\sim\dot{\gamma}^{3/5}a_v$) have similar scaling. Main differences in the limit of large *Ma* concern scaling with respect to σ and $\hat{\eta}$ and the dependence on copolymer diffusion unique to $Pe_{\sigma f}$.

4. Summary

The coalescence efficiency ε_v of immiscible polymer fluids containing copolymer surfactant was measured, as a function of temperature, copolymer molecular weight and copolymer concentration. At small Ca, the influence of Marangoni stress on drop trajectories is operative. In this regime, ε_v is independent of shear rate and drop size. In surfactant-free mixtures, this constant ε_v depends on the viscosity ratio. In mixtures containing surfactant, however, it correlates with $Ma\,Pe_{\rm eff}$ (see Eq. (14) and Fig. 6b) in the limit where interfacial concentration gradients are limited by diffusion-limited sorption. Since this sorption rate decreases with decreasing copolymer solubility, ε_v in this regime is reduced by decreasing temperature and increasing copolymer molecular weight (Figs. 4 and 6b).

At larger Ca, drops deform slightly and the influence of Marangoni stress on the drainage of a flattened film be-

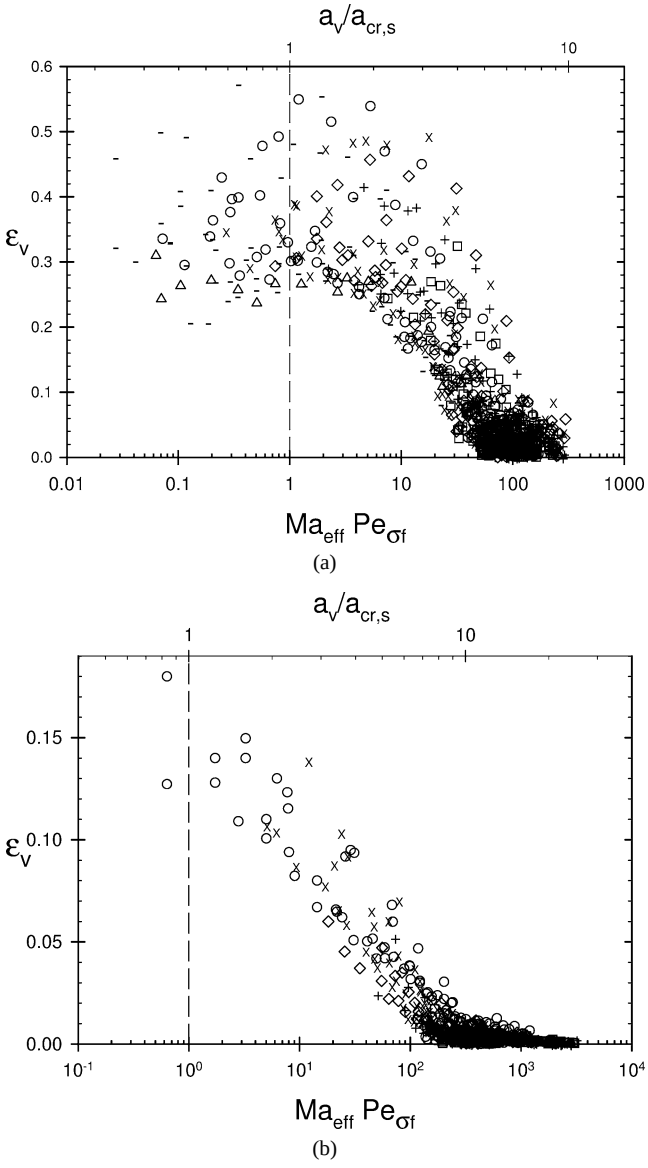

Fig. 8. The data of Fig. 5 is replotted here against $Ma_{\text{eff}}\,Pe_{\sigma f}$. To facilitate comparison with Fig. 5, the abscissa is also expressed as the volume-averaged dimensionless drop radius $a_v/a_{\text{cr},s}$, where $a_{\text{cr},s}$ is the length scale implicit in $Ma_{\text{eff}}\,Pe_{\sigma f}$, i.e., $a_v/a_{\text{cr},s} \equiv (Ma_{\text{eff}}\,Pe_{\sigma f})^{2/5}$.

tween drops is operative. ε_v decreases and approaches zero, leading to the arrest of coalescence. Whereas the arrest of coalescence in surfactant-free mixtures is governed by the parameter a_v/a_{cr}, in mixtures containing surfactant, the arrest occurs at different values of a_v/a_{cr}. Even though arrest occurs at much smaller deformations in mixtures containing surfactant, it is still associated with film drainage phenomena. The effect of surfactant is well described by the parameter $Ma_{\text{eff}}\,Pe_{\sigma f}$ (see Eqs. (17) and (18)). This parameter illustrates why the effect of surfactant on coalescence saturates even at small amounts of surfactant, because it reaches a constant value when *Ma* exceeds a characteristic value. This result provides a signature of the effect of interface *immobilization* on film drainage.

Similar behavior at both low and moderate Ca is expected for more insoluble surfactants, especially in the remobilization regime, where surfactant exchange with the bulk phase is important. In addition, at lower concentrations of insoluble surfactant, when interfacial diffusion is dominant, trajectory theory [9] is expected to hold at low Ca, and at higher Ca the theory for film drainage [10] (briefly described above) is expected to be valid. For high-molecular-weight block-copolymer surfactants, interfacial sorption kinetics may dominate at sufficiently high concentration. An important consequence of slow interfacial kinetics is that film rupture can be inhibited. Recent measurements that demonstrated the role of copolymer asymmetry are consistent with interfacial constraints that inhibit film rupture [40–44].

Acknowledgments

Partial financial support under NSF Grants CTS-9731502 and PHY99-07949 is gratefully acknowledged. We are grateful for helpful discussions with L.G. Leal. Calculations of drop coalescence efficiency by M.A. Rother and R.H. Davis are gratefully acknowledged.

References

[1] H. Wang, A.Z. Zinchenko, R.H. Davis, J. Fluid Mech. 265 (1994) 161–188.
[2] A.K. Chesters, Chem. Eng. Res. Design 69 (1991) 259–270.
[3] H. Yang, C.C. Park, Y.T. Hu, L.G. Leal, Phys. Fluids 13 (2001) 1087–1106.
[4] M.A. Rother, A.Z. Zinchenko, R.H. Davis, J. Fluid Mech. 346 (1997) 117–148. For more about the relationship of so-called dimensionless Hamaker parameters for general and glancing-angle collisions please see Section 3.4.
[5] M.A. Rother, R.H. Davis, AIChE J. 49 (2003) 546–548. See Eq. (6) for a definition of a_{cr}.
[6] M.A. Rother, R.H. Davis, Phys. Fluids 13 (2001) 1178–1190.
[7] A. Saboni, C. Gourdon, A.K. Chesters, J. Colloid Interface Sci. 175 (1995) 27–35.
[8] A.Z. Zinchenko, PMM J. Appl. Math. Mech. 44 (1980) 30–37.
[9] J. Blawzdziewicz, E. Wajnryb, M. Loewenberg, J. Fluid Mech. 395 (1999) 29–59.
[10] A.K. Chesters, I.B. Bazhlekov, J. Colloid Interface Sci. 230 (2000) 229–243.
[11] C.C. Park, Flow-Induced Drop Coalescence, Ph.D. thesis, Mechanical and Environmental Engineering, Univ. of California, Santa Barbara, 2002.
[12] L.G. Levich, Physicochemical Hydrodynamics, Prentice Hall, Englewood Cliffs, NJ, 1962.
[13] J.A. Ramirez, R.H. Davis, A.Z. Zinchenko, Int. J. Multiphase Flow 26 (2000) 891–920.
[14] J.A. Holbrook, M.D. Levan, Chem. Eng. Commun. 20 (1983) 273–290.
[15] J.A. Holbrook, M.D. Levan, Chem. Eng. Commun. 20 (1983) 191–207.
[16] Y.T. Hu, D.J. Pine, L.G. Leal, Phys. Fluids 12 (2000) 484–489.
[17] Y. Amarouchene, G. Cristobal, H. Kellay, Phys. Rev. Lett. 87 (2001) 206104.
[18] H. Mousa, T.G.M. van de Ven, Colloids Surf. 60 (1991) 39–51.

[19] B.E. Burkhart, P.V. Gopalkrishnan, S.D. Hudson, A.M. Jamieson, M.A. Rother, R.H. Davis, Phys. Rev. Lett. 87 (2001) 098304.
[20] D.L. Swift, S.K. Friedlander, J. Colloid Sci. 19 (1964) 621–647.
[21] M. Smoluchowski, Z. Phys. Chem. 92 (1917) 129–168.
[22] J.W. Ha, Y. Yoon, L.G. Leal, Phys. Fluids 15 (2003) 849–867.
[23] P. Linse, Macromolecules 27 (1994) 6404–6417.
[24] A. Luciani, M.F. Champagne, L.A. Utracki, J. Polym. Sci. Polym. Phys. 35 (1997) 1393.
[25] C. Huh, S.G. Mason, Colloid Polym. Sci. 253 (1975) 566.
[26] J.M. Rallison, Annu. Rev. Fluid Mech. 16 (1984) 45–66.
[27] G.I. Taylor, Proc. R. Soc. London Ser. A 138 (1932) 41–48.
[28] H. Yamane, M. Takahashi, R. Hayashi, K. Okamoto, H. Kashihara, T. Masuda, J. Rheol. 42 (1998) 567–580.
[29] A.N. Semenov, Macromolecules 25 (1992) 4967–4977.
[30] U. Jorzik, B.A. Wolf, Macromolecules 30 (1997) 4713–4718.
[31] L. Leibler, Macromolecules 15 (1982) 1283.
[32] A. Friday, D.R. Cooper, C. Booth, Polymer 18 (1977) 171–174.
[33] D.R. Cooper, C. Booth, Polymer 18 (1977) 164–170.
[34] M. Appel, G. Fleischer, Macromolecules 26 (1993) 5520–5525.
[35] M.C. Dalvi, T.P. Lodge, Macromolecules 27 (1994) 3487–3492.
[36] J.A. Ramirez, R.H. Davis, AIChE J. 45 (1999) 1355–1358.
[37] S.T. Milner, H.W. Xi, J. Rheol. 40 (1996) 663–687.
[38] V. Cristini, J. Blawzdziewicz, M. Loewenberg, J. Fluid Mech. 366 (1998) 259–287.
[39] S.D. Hudson, B.E. Burkhart, P.V. Gopalkrishnan, A.M. Jamieson, I. Manas-Zloczower, in: 13th International Congress on Rheology, Brit. Soc. Rheology, Cambridge, UK, 2000.
[40] J.R. Kim, A.M. Jamieson, S.D. Hudson, I. Manas-Zloczower, H. Ishida, Macromolecules 31 (1998) 5383–5390.
[41] J.R. Kim, A.M. Jamieson, S.D. Hudson, I. Manas-Zloczower, H. Ishida, Macromolecules 32 (1999) 4582–4587.
[42] A. Nandi, A. Mehra, D.V. Khakhar, Phys. Rev. Lett. 83 (1999) 2461–2464.
[43] J.R. Kim, S.D. Hudson, A.M. Jamieson, I. Manas-Zloczower, H. Ishida, Polymer 41 (2000) 9163–9168.
[44] S. Lyu, T.D. Jones, F.S. Bates, C.W. Macosko, Macromolecules 35 (2002) 7845–7855.
[45] S.D. Hudson, Phys. Fluids 15 (2003) 1106–1113.